# Non-equilibrium pattern formation in reactive channel flow

Christopher Hawkins


*Thesis submitted for the degree of Philosophiae Doctor*

*Department of Physics*
*Faculty of mathematics and Natural Sciences*
*University of Oslo, Norway*

*August 4, 2015*

*Series of dissertations submitted to the*
*Faculty of Mathematics and Natural Sciences, University of Oslo*
*No. 1691*

ISSN 1501-7710



Cover: Hanne Baadsgaard Utigard.
Print production: John Grieg AS, Bergen.

Produced in co-operation with Akademika Publishing.
The thesis is produced by Akademika Publishing merely in connection with the thesis defence. Kindly direct all inquiries regarding the thesis to the copyright holder or the unit which grants the doctorate.

# Contents

# Preface

This project was conducted as part of the Marie Curie ITN project MINSC (mineral scaling). MINSC focused on problems related to mineral growth in pipelines. Whilst many other partners in MINSC focus on the goechemical aspects of scaling this project studies the complex interaction between the mineral growth and the fluid dynamics of the pipeline flow.

A powerful tool in the human pocketknife of problem solving is the computer simulation. The ability to replicate and solve complex and otherwise unsolvable systems with perfect repeatability whilst providing an endless supply of information to what is happening is unparalleled by any other investigative technique. It is not perfect as one must first understand the rules and base equations which govern the system and accept that the accuracy is determined by the power of modern computers. A sample is therefore always required for comparison but beyond this the possibilities are almost endless.

The particular problem intended to be addressed by this work was that of mineral scale formation which refers to the deposition of solids upon surfaces which are exposed to fluids containing the solids (minerals) in question. This phenomenon would not be of such great concern to us if it were not for the fact that transport of such fluids is severely hindered by this process a most common occurrence we all know as pipe clogging. Hence we set out on a journey to simulate such a system from which we hoped to gain some understanding.

A valuable real life example of an extreme case of mineral scale formation takes place in the complex pipe network that makes up Hellishedi geothermal power plant in Iceland. Here hot mineral rich fluid is pumped from deep within the earth so as the extract the energy. This, however, results in a dramatic scaling problem as the minerals in the fluids solidify upon the pipe walls clogging the system over time.

Based upon an initial analysis of what was seen to be growing in the power plant it was assumed that a precipitation reaction, where dissolved substances solidify on solid surfaces, was responsible for the growth. Such a process is common to a wide variety of systems so that a model would provide an interesting, far reaching insight. The aim here, as with many investigations, was to understand the main processes which caused the observed structures which in this case were the

transport mechanisms bringing the dissolved substances into contact with the was so a reaction could take place. Whilst most of the processes could be explained and understood to a strong degree one mechanism stood out as not only being considerably more complex than the others but also having such a strong effect that it simply could not be ignored. Generated by the structure as it protruded from the boundary into the flow, turbulence would mix the fluid greatly enhancing the rate of surface growth. It was discovered that this effect could be so strong that it would dwarf many other mechanisms by several orders of magnitude.

Following the logical route an investigation into the nature of turbulence and its dependence upon the flow conditions then took place. This detailed examination would connect various aspects of turbulent flow for which the relationship was previously unknown.

A final detailed analysis of a real life mineral scaling sample taken from geothermal power plant in Iceland showed the structures consisted of a number of small particles which had aggregated together to form large structures. A model for this process was created where fluid flow was seeded with particles subject to classical collisions. Given the ability to stick together, these particles would produce the structures found in the power plant. The work was also able to provide detailed explanations of many of the observations made in the real life system.

# Chapter 1

# Introduction

The transport of fluid is one of the most important activities undertaken in the human world. Back to the dawn of civilization where channels were built to transport water for aggregation through to the modern world where oil is pumped through an extensive pipe systems which traverses continents on a global scale. It is an essential part of everyday life, but as with all endeavors we undertake we encounter problems and difficulties, many of which we have yet to overcome. Possibly the greatest problem facing fluid transport is that of pipe clogging. For one of a magnitude of reasons, solids can deposit upon the walls of a pipe or channel restricting the space and resisting the flow. Over-time the buildup of such solids becomes a major obstacle for the flow making the transport more and more laborious until the entire process is forced to shut down.

The buildup of solids, often referred to as surface growth processes, produce a variety of complex patterns. Patterns are an intrinsic part of nature which owe their existence to the origin of the universe. The big bang followed by cosmic inflation has left the universe in a state of non-equilibrium. Most important in pattern formation are the instabilities which result from such a system of non-equilibrium. These instabilities push a system to move from one state to another from which even a simple system will produce complex patterns. A perfect example of this style of solidification pattern is the snowflake. Here cool water vapor in air will be absorbed onto the surface of the snowflake changing state from liquid to solid and building the shapes we eventually observe.

Non-equilibrium pattern formation entered the physics mainstream in the lat-

ter part of the 20th century. In 1980 Langer released his benchmarking paper [14] providing a strong mathematical framework for the patterns formed in solidification systems. Starting from this initial work, progress over the following decades has given such insight so as to make the complex shape of the snowflake one of the best understood non-equilibrium patterns.

The solidification process present in snowflakes is similar in many respects to solidification in geological systems. It is common to find fluids with dissolved minerals or even suspended particles which will develop instabilities in their state after the system is subject to a change of conditions. It is these fluids that are the most troublesome to transport as moving them is often the direct cause of a change in conditions. Pumping fluid out of the ground is a widespread example due to the temperature and pressure differences between the earths surface and the underground reservoir from which the fluids are moved. This is not only a man made cause as many natural systems also involve the transport of fluids from one region to another.

Unlike our understanding of snowflake formation the addition of flow adds considerable complexity to the system. It is this dynamic interplay between growth and flow that produces many of the beautiful pattern structures seen in geological systems. Some striking examples the terraces which form as mineral rich fluid flows down an incline. Here mineral deposition causes the build-up of an extensive terrace network consisting of a series of ridges that trap water in pools. Similar flows which come directly up from the ground produce symmetric dome structures whilst commonly imaged stalactites and stalagmites form as geological fluids fall off ceilings such as those found in caves [19].

In this thesis we study surface growth reactions that take place within channel flow, leading to many beautiful patterns but also causing eventual clogging, hindering flow transport. As such this work is a cross disciplinary project between physics, regarding flows and pattern formation, and geology of the minerals and particles which solidify within geological systems. Many of the samples and systems we study will be of a geological nature, such as the transport of geothermal fluid within power plants, this shall then be approached from a physics point of view with simulations, analysis and theoretical predictions stemming from physics.

# Chapter 2

# Material transport

For solids to build up it is required that these solids, or the components which make them, exist within a fluid. Depending on the nature of these solids two main approaches to deposition occur. In the cases where the solid is contained within the fluid as either dissolved molecules or as a series of components which react to form a solid the process is usually known as precipitation.

The alternative to this sees larger particles aggregate upon collision with one another, eventually causing the build-up of larger and larger structures in a manner described as ballistic aggregation. The core difference here is that for the case of precipitation solids will only start to build if it is energetically favorable to do so. This criterion is most commonly achieved if the solution is supersaturated with respect to the solid components.

Supersaturation is the point at which the dissolved solid components contained within the fluid exceeds the maximum amount of such components that could be normally dissolved within the solution under its current circumstances. This maximum quantity (solubility), as measured by experiments, is dependent upon temperature and in almost all circumstances the solubility increases with increasing temperature. If a solution were therefore to be cooled it can easily become supersaturated resulting in the aforementioned precipitation. This is not necessarily only dependent of changes in heat but also either pressure or volume as seen through the ideal gas law.

In the case of ballistic aggregation there is no such quality as supersaturation and the density of particles is almost irrelevant. What is important however is that

these particles are capable of sticking to one another in order to build up structures larger than themselves. Unlike precipitation whose morphology is determined by the crystalline structure of the solids, ballistic aggregation is dependent upon the size and type of the particles themselves. This is due to the fact that despite merging to form a larger structure the individual particles continue to remain distinctive and isolated from one another.

Common to all these surface growth systems are a number of core processes. These processes are the transport mechanisms of the material from which the solids are built to the surface of the growing structures. The two most widely encountered transport processes are advection and diffusion.

## 2.1 Diffusion

On a large scale diffusion can be seen as the spreading of a substance from regions of high concentration to regions of low concentration in a manner that evens out the concentration field. it is often refered to as the movement of a substance down the concentration gradient. Like many processes its origins lie on the microscale as a type of apparent random motion known as Brownian motion. Particles which are contained within a gas or liquid continuously collide with the fast moving fluid molecules causing them to jump around in a seemingly random fashion. What is important is that this occurs for particles of all sizes due to instantaneous inhomogenities in the number of fluid particles colliding from each direction. However, the magnitude of the effect is therefore usually less for larger particles as mass tends to increase as particles get larger. The deposition of solid particles upon a surface is equivalent to removing these particles from the fluid and can hence be described as a sink continuously removing the solid from the solution. Here diffusion as a transportation process plays its most important role as it seeks to move the solution down the concentration gradient towards the surface of the growing structure. The general equation for diffusion is derived primarily from the assertion that a substance flows from a region of high concentration to one of low concentration. If this is the case then at the point where the system reaches

steady state the flux $J$ from one region to the other can be written as

$$J = -D\frac{\partial L}{\partial x} \tag{2.1}$$

Where $L$ here describes the concentration field of some substance and $D$ is simply a constant. This is known as Fick's first law. More importantly, this equation can be used to derive the change of concentration of property $L$, which can be written as

$$\frac{\partial L}{\partial t} = -D\frac{\partial^2 L}{\partial x^2} \tag{2.2}$$

and is known as Fick's second law.

## 2.2 Advection

Advection is caused by the bulk motion of fluids and acts to push particles along the fluid streamlines. The magnitude of advection can often be significant and hence the transport effectiveness for many real life flows will far exceed that of diffusion. The equations surrounding advection can be derived simply by considering conservation of a substance that is moved by some velocity field $\mathbf{u}$. By defining the volume $\Omega$, and the surface surrounding it $\partial\Omega$, initially one starts with the Reynolds transport theorem for a property $L$

$$\frac{d}{dt}\int_{\Omega} L dV = -\int_{\partial\Omega} L\mathbf{u}\cdot\mathbf{n}dA - \int_{\Omega} Q dV \tag{2.3}$$

The left hand side is the rate of change of $L$ whilst the right hand side has to terms, the flux term $\int_{\partial\Omega} Lu\cdot ndA$ which results from the flow of $L$ and $\int_{\Omega} QdV$ which is the source/sink term. To this we apply the divergence theorem to the first term on the right hand side converting the surface integral to a volume integral giving the equation in the form:

$$\frac{d}{dt}\int_{\Omega} L dV = -\int_{\Omega} \nabla\cdot(L\mathbf{u})dV - \int_{\Omega} Q dV \tag{2.4}$$

Finally, by applying Leibniz's rule we arrive at the general form for the continuity equation.

$$\frac{dL}{dt} = -\nabla \cdot (L\mathbf{u}) - Q \tag{2.5}$$

The main difference in complexity between advection and diffusion is the velocity field causing the advection itself. In the case of fluids it shall be seen that this velocity field is not trivial to calculate.

## 2.3 Navier-Stokes

Fluid flows are represented by the Navier-Stokes equations, a set of complete continuous equations that completely defines the motion of fluids without inaccuracy. These flows are the factor responsible for advection as described above. The Navier-Stokes equations are derived from basic conservation and continuity equations relating to mass and momentum.

#### Conservation of mass

Applying the conservation equation, as derived for advection, to mass or rather density (the intensive equivilent) we gain

$$\frac{d\rho}{dt} = -\nabla \cdot (\rho\mathbf{u}) \tag{2.6}$$

where we have set the source term to zero ($Q = 0$) which is perfectly valid for the general case where mass is not added or removed from the system. In the case of incompressible flow where $\rho$ is a constant the divergence of the velocity field becomes zero

$$\nabla \cdot \mathbf{u} = 0 \tag{2.7}$$

#### Conservation of momentum

From Newton's second law we have that

$$\mathbf{F} = m\mathbf{a} \tag{2.8}$$

which, assuming a body force $\mathbf{b}$ can be rewritten in terms of the momentum as

$$\mathbf{b} = \rho \frac{d\mathbf{u}}{dt} \tag{2.9}$$

Applying the chain rule to this derivative

$$\mathbf{b} = \rho(\frac{\partial \mathbf{u}}{\partial t} + \mathbf{u} \cdot \nabla \mathbf{u}) \tag{2.10}$$

The body force is usually assumed to consist of two componets, fluid stresses and external forces, which can be written as $b = \nabla \cdot \sigma + f$ where $\sigma$ is the stress tensor and $f$ the external forces. The stress tensor can be written in terms of the stress deviator tensor $T$ and the pressure $P$

$$\sigma = -PI + T \tag{2.11}$$

where $I$ here denotes the identity matrix. Substituting this into the conservation equation we gain the most general form of the Navier-Stokes

$$\rho(\frac{\partial \mathbf{u}}{\partial t} + \mathbf{u} \cdot \nabla \mathbf{u}) = -\nabla \cdot P + \nabla \cdot T + \mathbf{f} \tag{2.12}$$

It can be found that the divergent stress term can be expanded to give

$$\nabla \cdot T = \mu \nabla^2 \mathbf{u} \tag{2.13}$$

which when substituted provides the most familiar form of the Navier-Stokes

$$\rho(\frac{\partial \mathbf{u}}{\partial t} + \mathbf{u} \cdot \nabla \mathbf{u}) = -\nabla \cdot P + \mu \nabla^2 \mathbf{u} + \mathbf{f} \tag{2.14}$$

The complex non-linear term here can be seen as the second on the left hand side $u \cdot \nabla u$. This term is often thought of as the advection of the velocity field along itself and this is responsible for the chaotic nature of flows known as turbulence. It is important to realize however that flows will often reach a steady state for a specific prescribed boundary condition. Whilst the flow may continue to fluctuate on short timescales due to the turbulence, over longer timescales average values for the velocity field will converge to a steady point. Such averages allow us to

predict the progress of the system without being overly concerned about its intricate complexities.

One may naively think that when a steady state has been reached it is possible to use average values to fully predict the solidification process based upon advection and diffusion. In many other static systems this may be true but this oversimplification neglects the most important component of the growing solidification process, namely the changing boundary conditions. As the boundaries move due to growth so do the flow conditions altering the streamlines and induction of turbulence. Further they move the sink/source associated with the solidification altering the concentration field. Hence the magnitude of advection and diffusion is changed throughout the system which then in turn affects the growth rate across the surface of the growth altering the changing geometry. This continuous feedback loop defines the complexity faced when dealing with such systems. Hence we must turn to simulations in order to gain a better insight into the general rules surrounding solidification in flow.

# Chapter 3

# Numerical Simulations

Scientists have turned to simulations to replicate otherwise unsolvable problems resulting from the complex nature of almost all systems. The first large scale use of computer simulations occurred during World War II within the infamous Manhattan Project. To model the nuclear detonation, simulations of hard spheres were run through a Monte-Carlo algorithm allowing scientists to correctly design weapons that worked first time [25]. In the post-war world new military technology designed for the war emerged for the civilian world, among them simulations would radically change the way complex problems were to be solved. In the 1950s the first commercially designed computers arrived and the age of numerical modeling begun. However, plagued by problems it was not until the 1960s where developments from IBM brought computing into the mainstream and over the next few decades a surge of pioneering development advanced simulations so that by the mid 1980s they were at the forefront of scientific research. Since then computing power has exponentially increased with dropping cost giving such widespread availability that almost every person on the planet can run complex simulations using even the most basic computers available.

This is where this work in understanding and predicting pipe clogging begins with its viral replication within the numerical world. What follows is a theoretical outline for the models used to simulate surface growth and flow along with some of the numerical techniques used to solve many of the resulting equations.

Figure 3.1: Snapshot of growth in the phase-field model where a single seed is placed with a supersaturated solution and allowed to grow

## 3.1 Phase-field model

The biggest obstacle encountered when modeling continuous systems with a changing interface (such as precipitation) within a computer is the tracking of the interface itself. To do this without the use of certain methods (phase field, level set) requires the model to search the entire system to first find each point of the interface and often to determine the location of the interface surrounding each point. This must take place before any calculation is made which is computationally expensive and hence time consuming, something we wish to avoid. The phase-field model bypasses this by making the interface an inherent part of the equations which govern the system allowing a computer to simply solve the equations without requiring any knowledge of the actual interface location. The idea of the diffuse interface was first developed by van der Waals in the 1800s [29], later Cahn and Hilliard [2] used this to determine the free energy of the interface within a system with a varying composition paving the way to the phase field model. The first phase field simulations applied the Cahn-Hilliard equations to the situation of pure melts as undertaken initially by Collins and Levine [4] and soon after by Langer [15] in the mid 1980s. Since then the phase field approach

has been used to simulate a magnitude of moving interface problems including precipitation (e.g. [31]) whose formulation shall be drawn upon here.

### 3.1.1 Reaction kinetics

Precipitation is defined as the creation of a solid taking place within a solution containing one or more dissolved solid components. Here a reaction occurs at a solid-liquid interface where substances are transported from one phase to the other. Whilst some precipitation process can involve a complex sequenced of reactions, the simplest is a single component first order reaction which, despite its simplicity, can provide significant insight into the nature of precipitation. For this simple case the flux of the solute at the interface can be described with linear kinetics as

$$D\nabla C \cdot \mathbf{n} = k(C - C_e) \tag{3.1}$$

where $D$ is the diffusion coefficient, $C$ is the concentration of the dissolved solute, $n$ the normal to the interface, $k$ the reaction rate and $C_e$ the concentration at equilibrium.
The velocity of the interface, $v_s$, results from a volume calculation and can then be written as

$$v_s = \frac{k}{\rho_s}(C - C_e) \tag{3.2}$$

Here $\rho_s$ is the mass density of the solid. This equation implies mass conservation of the moving interface.
In addition the solute dissolved within the liquid will undergo diffusion which takes the form.

$$\frac{\partial C}{\partial t} = D\nabla^2 C \tag{3.3}$$

Diffusion within the solid phase is assumed to be negligible.
These equations can be rewritten in terms of the normalized concentration to provide the time dependent concentration field which governs the liquid

$$\frac{\partial c}{\partial t} = D\nabla^2 c + v_s \nabla c \cdot \mathbf{n} \tag{3.4}$$

where $c = (C - C_e)/C_e$ is the normalized concentration.

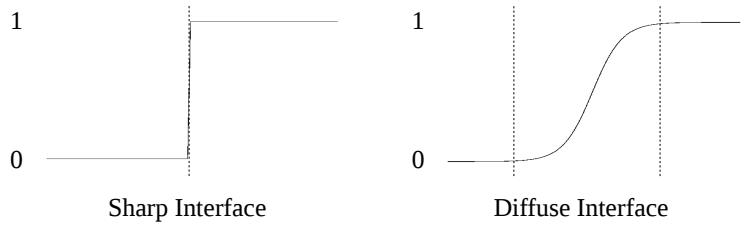


Figure 3.2: A cut through the interface showing the variation of phase-field value $\phi$ as it trasitions from liquid ($\phi = 0$) to solid ($\phi = 1$). Left, a sharp interface similar to that found in real systems. Right, the interface within the phase-field model with a finite thickness as the phase-field value transitions from liquid to solid.

### 3.1.2 Diffuse interface

We begin by defining a phase variable $\phi$ which describes the phase continuum and takes values of $\phi = -1$ for pure solid and $\phi = 1$ for pure liquid phases, phi is also continuous and can take any values between the two extremes. Figure 3.2 demonstrates a typical diffuse interface as $\phi$ gradualy varies from liquid to solid phases. The phase field model is then based upon the idea of free energy and we assume that the free energy associated with $\phi$ can be written as:

$$F = \int_V \left(g(\phi, \nabla\phi) + f(\phi, c)\right) dV \tag{3.5}$$

where $g(\phi, \nabla\phi)$ is the energy due to inhomogeneity due to gradients in the phase field, $f(\phi, c)$ is the free energy density and $dV$ is the volume element.

Giving $g(\phi, \nabla\phi)$ the form $g(\phi, \nabla\phi) = (1/2)\varepsilon^2|\nabla\phi|^2$ allows us to write a full set of time evolution equations for the system as:

$$\frac{\partial\phi}{\partial t} = \frac{\partial F}{\partial\phi} = \frac{1}{\tau}\varepsilon^2\nabla^2\phi + \frac{\partial f(\phi, c)}{\partial\phi} \tag{3.6}$$

for the phase field, and

$$\frac{\partial c}{\partial t} = D\nabla^2 c + A\frac{\partial\phi}{\partial t} \tag{3.7}$$

for the concentration field. From the phase equation for $\phi$ it can be seen that the first term resembles a diffusive term, it acts precisely is this manner diffusing the interface and giving it a thickness depending on $\epsilon$ which is usually referred to as the interface thickness. $\tau$ controls that rate at which $\phi$ is able to change and is physically related to the mobility of the systems particles. For the concentration field the first term is the standard diffusive term controlling diffusive transport. In addition a term is gained based upon the rate of change of $\phi$ which is the equivalent of a source term adding or subtracting to the concentration field as substances precipitate from the solution to the solid.

This is the most basic form of the phase field model which now removes the need for explicit interface traking as the equations are simply solved throughout the system.

### 3.1.3 Zero width

In order to define true precipitation reaction kinetics we must make further definitions and finally rework the equations so that in the limit of the interface width going to zero the original equations defined for reaction kinetics are precisely reproduced. First, note that the phase equations are defined in terms of cartesian coordinates rather than with respect to the interface normal. This results in an error associated with the curvature which can quickly be discovered through a transformation to normal coordinates which to first order reads $\nabla^2 = \partial^2/\partial n^2 + \kappa\partial/\partial n$. This reveals the additional term which must then be subtracted to cancel it from the equations.

$$\tau\frac{\partial\phi}{\partial t} = \varepsilon^2\nabla^2\phi + (1-\phi^2)(\phi - \lambda c) - \varepsilon^2\kappa\left|\nabla\phi\right| \tag{3.8}$$

Here $\kappa$ is the curvature given by $\kappa = \nabla\cdot(\nabla\phi/|\nabla\phi|)$.

The free energy density $f(\phi)$ takes the form of a double well potential where at equilibrium the probability of precipitation is equal to the probability of dissolution. As the concentration increases the probability of precipitation should also increase, in the case where this increase is linear the free energy density takes the form:

$$f(\phi, c) = (-\phi^2/2 + \phi^4/4) + \lambda c(\phi - \phi^3/3) \tag{3.9}$$

$\lambda$ is the coupling constant which determines the gradient of increase as the magnitude of $c$ becomes larger. This can be substituted into the phase equation to produce its final form

$$\tau\frac{\partial\phi}{\partial t} = \varepsilon^2\nabla^2\phi + (1-\phi^2)(\phi - \lambda c) - \varepsilon^2\kappa\,|\nabla\phi| \tag{3.10}$$

In its most basic form the equation for the time evolution of concentration is:

$$\frac{\partial c}{\partial t} = D\nabla^2 c + A\frac{\partial\phi}{\partial t} \tag{3.11}$$

where, as mentioned, the final term provides the source term due to the transport of material from one phase to another. If the sharp interface limit ($\varepsilon \to 0$) is taken for the phase equation we find that $A = \rho/2C_e k$. However, in order to ensure the boundary condition given for the reaction kinetics are fulfilled we must add several additional terms. The first term is an additional source term which accounts for the fact that precipitation of a solid with specific density $\rho$ is related to a non-zero concentration, the other term must generate the concentration discontinuity. This leads to:

$$\frac{\partial c}{\partial t} = D\nabla^2 c + A_1\frac{\partial\phi}{\partial t} + A_2\frac{\partial\phi/\partial t}{|\nabla\phi|}(D\nabla^2\phi - \frac{\partial\phi}{\partial t}) \tag{3.12}$$

From here we wish to recreate the appropriate reaction kinetics. Transform to curvilinear co-ordinate system [$\nabla^2 = \partial^2/\partial n^2 + \kappa\partial/\partial n$]

$$\tau\frac{\partial\phi}{\partial t} = \epsilon^2\frac{\partial^2\phi}{\partial n^2} - \frac{\partial f}{\partial\phi} \tag{3.13}$$

$$\frac{D}{v_n}\frac{\partial^2 c}{\partial n^2} + (\frac{D\kappa}{v_n} + 1)\frac{\partial c}{\partial n} = A_1\frac{\partial\phi}{\partial n} + A_2\frac{\partial\phi}{\partial n} + A_2 D(\frac{\partial^2\phi}{\partial n^2} + \kappa\frac{\partial\phi}{\partial n}) \tag{3.14}$$

Imposing the boundary conditions,

$$v_n = \rho\beta c$$
$$n\cdot\nabla c = (k/D)\cdot c$$

($\beta = 1/\rho$)

integrate by $dn$ and take sharp interface limit (interface becomes a step function as $\varepsilon \to 0$)

$$\frac{D}{v_n}\frac{\partial c}{\partial n}|_-^+ + (\frac{D\kappa}{v_n} + 1)c|_-^+ = A_1\phi|_-^+ + A_2\phi|_-^+ + A_2 D(\frac{\partial \phi}{\partial n}|_-^+ + \kappa\phi|_-^+) \tag{3.15}$$

We now gain for $A_1$ and $A_2$:

$$A_1 = \frac{1}{2\beta}$$
$$A_2 = \frac{v_0}{2\beta k}$$

For concentration the equation now becomes

$$\frac{\partial c}{\partial t} = \frac{D}{x_0^2/t_0}\nabla^2 c + \frac{1}{2\beta}\frac{\partial \phi}{\partial t} + \frac{v_0}{2\beta k}\frac{\partial\phi/\partial t}{|\nabla\phi|}(\frac{D}{x_0^2/t_0}\nabla^2\phi - \frac{\partial\phi}{\partial t}) \tag{3.16}$$

### 3.1.4 Dimensionless form

Initially we propose a series of scaling variables $x_0, t_0$, and $v_0$ and further impose the condition $x_0/t_0 = v_0$ then

$$\frac{D}{x_0^2/t_0} = \frac{D}{x_0 v_0} = \frac{1}{P_e}$$
$$\frac{x_0 k}{D} = D_a$$

Here $P_e$ the Peclet number is the ratio between advection (due to the fluid motion) and diffusion. $D_a$ Damkoler number is the ratio between reation and diffusion. The equation for concentration now reads

$$\frac{\partial c}{\partial t} = \frac{1}{P_e}\nabla^2 c + \frac{1}{2\beta}\frac{\partial \phi}{\partial t} + \frac{P_e}{2\beta D_a}\frac{\partial\phi/\partial t}{|\nabla\phi|}(\frac{1}{P_e}\nabla^2\phi - \frac{\partial\phi}{\partial t}) \tag{3.17}$$

where $v_0/k = P_e/D_a$ is the ratio between advection and reaction.

For the phase in dimensionless form, using the above we now have

$$\frac{\partial \phi}{\partial t} = \frac{\epsilon^2}{x_0^2}\frac{t_0}{\tau}\left(\nabla^2\phi - \kappa|\nabla\phi|\right) - \frac{t_0}{\tau}\frac{\partial f}{\partial \phi} \tag{3.18}$$

We make the new definition:

$$P_{er} = \frac{x_0 v_r}{D} = \frac{x_0^2/\tau}{D}$$
$$x_0/\tau = v_r$$

$P_{er}$ is now the ratio of interface advection (due to reaction) and diffusion. Then:

$$\frac{t_0}{\tau} = \frac{P_{er}}{P_e}$$

Is the ratio of advection due to reaction and advection due to bulk fluid motion. Finally for $\phi$

$$\frac{\partial \phi}{\partial t} = \frac{P_{er}}{P_e}\left[\frac{\epsilon^2}{x_0^2}\left(\nabla^2\phi - \kappa|\nabla\phi|\right) - \frac{\partial f}{\partial \phi}\right] \tag{3.19}$$

The final constant $\epsilon/x_0$ describes the sharpness of the interface.

### 3.1.5 Finite difference

The finite difference method allows the estimation of gradients within a discrete system such as those encountered within numerical simulations where arrays of numbers exist rather than continuous variables. There are three commonly used difference schemes:
The forwards difference

$$f'(x) \sim \frac{f(x+\Delta x) - f(x)}{\Delta x} \tag{3.20}$$

The backwards difference

$$f'(x) \sim \frac{f(x) - f(x-\Delta x)}{\Delta x} \tag{3.21}$$

The central difference

$$f'(x) \sim \frac{f(x+\frac{1}{2}\Delta x) - f(x-\frac{1}{2}\Delta x)}{\Delta x} \tag{3.22}$$

Where $\Delta x$ is some spacial increment. From this starting point it is trivial to derive higher order differences such as the second order central difference:

**Phase-field with finite difference**

To determine the finite difference correspondence of various differentials requires a combination of differentials in various directions. For greater accuracy within the model off axis points, sometimes referred to as next nearest neighbors are also considered. For the various differentials:

$$\nabla^2\phi_{i,j} = \frac{\phi_{i+1,j} + \phi_{i-1,j} + \phi_{i,j+1} + \phi_{i,j-1} - 4\phi_{i,j}}{ds^2} \tag{3.23}$$

$$|\nabla\phi|_{i,j} = \frac{1}{2ds}\sqrt{(\phi_{i+1,j} - \phi_{i-1,j})^2 + (\phi_{i,j+1} - \phi_{i,j-1})^2} \tag{3.24}$$

$$\begin{aligned}\nabla \cdot (\frac{\nabla\phi}{|\nabla\phi|})_{i,j} = \\ \frac{1}{ds}[&\frac{\phi_{i+1,j} - \phi_{i,j}}{\sqrt{(\phi_{i+1,j} - \phi_{i,j})^2 + (\phi_{i+1,j+1} + \phi_{i,j+1} - \phi_{i+1,j-1} - \phi_{i,j-1})^2/16}} \\ &- \frac{\phi_{i,j} - \phi_{i-1,j}}{\sqrt{(\phi_{i,j} - \phi_{i-1,j})^2 + (\phi_{i-1,j+1} + \phi_{i,j+1} - \phi_{i-1,j-1} - \phi_{i,j-1})^2/16}} \\ &+ \frac{\phi_{i,j+1} - \phi_{i,j}}{\sqrt{(\phi_{i,j+1} - \phi_{i,j})^2 + (\phi_{i+1,j+1} + \phi_{i+1,j} - \phi_{i-1,j+1} - \phi_{i-1,j})^2/16}} \\ &- \frac{\phi_{i,j} - \phi_{i,j-1}}{\sqrt{(\phi_{i,j} - \phi_{i,j-1})^2 + (\phi_{i+1,j-1} + \phi_{i+1,j} - \phi_{i-1,j-1} - \phi_{i-1,j})^2/16}}]\end{aligned} \tag{3.25}$$

In all the above, $ds$ is the lattice spacing and, $i, j$ represents the lattice position.

**Time stepping**

The finite difference scheme needs not only apply to spacial derivatives, it is equally valid for the temporal terms. However, in this case rather than calculating the value of the gradient the unknown value of $f$ at the next time step i.e. $f(t + \Delta t)$ is desired with $\Delta t$ being some time increment. Using the forwards finite difference and rearranging the equation used to proceed the system forward in time is acquired:

$$f(t + \Delta t) = \frac{1}{2} \left( f(t - \Delta t) + f(t) \right) \Delta t \tag{3.26}$$

This is often refered to as the forwards Euler method.

## 3.2 Lattice Boltzmann model

The Navier-Stokes equations are a complete continuous description of fluids, if it were possible to solve these equations a complete description of the flow of fluids would be gained. Due to their non-linearity however, it is not possible to solve all but the most simple systems and therefore numerical modeling must be used to reproduce the majority of flows. Numerical modeling does however have its limits, most notable in this case is the fact that a continuous set of equations cannot be completely solved using a discrete set of methods. The lattice Boltzmann method uses a different approach where instead of starting with the continuous Navier-Stokes equations begins with discrete particles, free-streaming within cloud, and at infrequent times interacting through collisions.

The lattice Boltzmann model originated from a very simplistic type of model known as Lattice Gas Cellular Automata (LGCA). Derived in 1986 by Uriel Frisch, Brosl Hasslacher and Yves Pomeau [28] in this model gases were simulated by a number of particles which moved upon a discrete lattice. Unlike the lattice Boltzmann model however, when two particles collided within LGCA they would follow a set of collision rules rather then a statistical relaxation process. These rules obeyed nothing more then conservation laws on the microscopic level but surprisingly were capable of producing macroscopic fluid motion. It did however suffer from a number of problems regarding noise and its extension to 3D

[5]. In 1988 McNamara and Zanetti [18] decided to replace individual particles in the system with mean occupations hence removing the noise associated with single particle statistics. The model was still limited to a single viscosity as it continued to use the collision rules of LGCA. Shortly after Higuera and Jimenez [11] proposed the idea of a linear collision operator allowing certain parameters to be adjusted hence affecting the viscosity. Later the inclusion of a specific type of linear operator (Bhatnagar-Gross-Krook [1]) with a single relaxation time that could be directly related to the fluid viscosity was implemented producing the model most commonly known today (often referred to as LBGK).

### 3.2.1 Boltzmann statistics

We begin with the idea of thermal equilibrium. When two bodies of different temperature come in thermal contact, heat, energy in transit, will flow between the two. Thermal equilibrium is reached when the total heat flow between the two bodies becomes zero. If the energy of the two systems is $E_1$ and $E_2$ then the total energy of the system $E = E_1 + E_2$ is fixed assuming the systems cannot exchange energy with anything else. The micro-states of the system (the configuration of the systems smallest denominators) can be calculated from the values of energy. If the first system can be in any one of $\Omega_1(E_1)$ micro-states and the second in $\Omega_2(E_2)$, then the total number of micro-states for the system is $\Omega_1(E_1)\Omega_2(E_2)$. The systems are allowed to exchange energy until they have come into thermal equilibrium then the system will be in a configuration which maximizes the number of micro-states. By maximizing the the number of micro-states we arrive at the following expression

$$\frac{dln\Omega_1}{dE_1} = \frac{dln\Omega_2}{dE_2} \tag{3.27}$$

and applying the fact that both systems now have the same temperature $T$ we can define the temperature by

$$\frac{1}{k_B T} = \frac{dln\Omega}{dE} \tag{3.28}$$

where $k_B$ is the Boltzmann constant. Let us now assume a case where one of the systems is negligible in size compared to the other. If the total system has energy $E$ and the small system attains energy $\epsilon$ the large system, considered to be a reservoir, will then have energy $E - \epsilon$. The variable of interest is the probability

$P(\epsilon)$ that the small system has energy $\epsilon$. This probability is proportional to the number of micro-states of the entire system which is now

$$P(\epsilon) = \Omega_1(E - \epsilon) \tag{3.29}$$

since the number of micro-states of the small system is equal to 1. This equation can be solved giving the famous Boltzmann distribution

$$P(\epsilon) = e^{-\epsilon/k_B T} \tag{3.30}$$

### 3.2.2 Gas kinetics

For gases we wish to determine the probability distribution of momentum within the system. Momentum can be written in terms of the energy as

$$E = p^2/2m \tag{3.31}$$

which we can insert into the Boltzmann distribution and normalize by integrating over a spherical shell to provide

$$f(p) = \frac{1}{(2\pi m k_B t)^{3/2}} e^{-p^2/2mk_B T} \tag{3.32}$$

in the case of a gas however we can rewrite this in terms of the density of a small volume element to gain

$$f(p) = \frac{1}{(2\pi R t)^{3/2}} e^{-u^2/RT} \tag{3.33}$$

### 3.2.3 Discretisation onto a lattice

The lattice Boltzmann model is a large simplification of real gases. It arises due to the fact that simulating a true cloud of gases, for which one mole consists of $10^{23}$ particles, requires computing power far beyond the most powerful computers available today. Therefore not only is this not practical but also not necessary since we are not interesting in the micro properties of the fluid only in the large

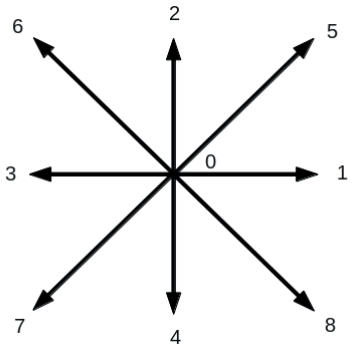


Figure 3.3: Lattice representaion of orientaions. In this model the D2Q9 lattice is used (2 dimensions 9 directions), $i$ = 0 represents particles at rest.

scale macro properties. To this extent we simplify the cloud of particles in a number of ways. The particles are restricted to moving at only one speed in a specific number of directions ($e_i$), Figure 3.3 shows a typical setup for the descrete set of directions. With careful choice of speeds, directions and time-step this allows a simulated setup where particles move from one lattice point to the next upon a regular grid within a time step. The second simplification is the grouping of all particles traveling in a specific direction into one cloud of particles whose collisions are now handled using Boltzmann statistics which work on averages of microscopic states. The lattice Boltzmann method now proceeds by attempting to relax the system towards local equilibrium as defined by the Boltzmann distribution. First however, the equations have to be recast into their discrete forms. For a single particle distribution we have

$$f(\mathbf{x}, t) = w_i f(\mathbf{x}, \mathbf{e}_i, t) \tag{3.34}$$

Here $w_i$ are weighting functions. At each grid point the total mass and velocity of the fluid can be inferred by summing the contributions from each particle function.

The velocity $u$ and the density $\rho$ are hence calculated as.

$$\rho = \sum_i n_i$$
$$\mathbf{u} = \frac{1}{\rho} \sum_i n_i \mathbf{e}_i$$

Finally the equilibrium distribution for the discritised system becomes

$$f_i^{eq} = \frac{1}{(2\pi Rt)^{3/2}} e^{-(\mathbf{e}_i - \mathbf{u})^2 / RT} \tag{3.35}$$

This expressions contains an exponential function which is very expensive to calculate numerically and for this reason the term is expanded around $u = 0$ providing the discrete equilibrium distribution

$$n_i^{eq} = w_i \rho (1 + \frac{3 e_{ia} u_a}{c^2} + \frac{9 e_{ia} e_{ib} u_a u_b}{2c^4} - \frac{3 u_a u_a}{2c^2}) \tag{3.36}$$

$\mathbf{u}$ is the velocity, $a$ and $b$ take the values $1, 2$ representing $x, y$ as before, summation is implied over indicies $a$ and $b$. The weights $w_i$ are determined by ensuring that the velocity moments (calculated from summing the particle functions as above) in the discrete case are equal to the original continuous case. This is done by solving the moments up to second order. In the case of the 2D system with 9 directions the weights are calculated as

$$w_0 = 4/9$$
$$w_{1,2,3,4} = 1/9$$
$$w_{5,6,7,8} = 1/36$$

The system will now relax to equilibrium at a rate controlled by the properties of the fluid then the evolution of the particle functions with time proceeds as.

$$n_i(x_a + c_{ia}, t + \Delta t) = n_i(x_a, t) - \frac{1}{\tau}[n_i(x_a, t) - n_i^{eq}(x_a, t)] \tag{3.37}$$

where a relaxation parameter $\tau$ determines the relaxation rate.

## Reproducing the Navier-Stokes

In order to verify that the lattice Boltzmann method recreate the required Navier-Stokes equations and to determine how the relaxation parameter relates to the properties of the fluid it is necessary to make the link between the numerical and continuous description.

The starting point is the Taylor expansion of the lattice Boltzmann equation which gives

$$\frac{1}{\tau}[n_i(x_a,t) - n_i^{eq}(x_a,t)] = \sum_{k=0}^{\infty} \frac{\Delta t}{k!} D_i^k n_i(x_a,t) \tag{3.38}$$

where the total derivative has been defined as

$$D_i = \frac{\partial}{\partial t} + ce_{ia}\partial_a \tag{3.39}$$

Defining $n^{(k)}(x_a,t)$ as the approximation of $n$ to order $k$ the first three orders are then

$$\begin{aligned}
n_i^{(0)}(x_a,t) &= n_i^{eq}(x_a,t) \\
n_i^{(1)}(x_a,t) &= n_i^{eq}(x_a,t) - \tau\Delta t D_i n_i^{eq}(x_a,t) \\
n_i^{(2)}(x_a,t) &= n_i^{eq}(x_a,t) - \tau\Delta t D_i n_i^{(1)}(x_a,t) - \tau\frac{\Delta t^2}{2} D_i^2 n_i^{eq}(x_a,t)
\end{aligned}$$

From here the equation for $n_i^{(1)}$ is substituted into the equation for $n_i^{(2)}$ giving

$$n_i^{(2)}(x_a,t) = n_i^{eq}(x_a,t) - \tau\Delta t D_i n_i^{eq}(x_a,t) - \tau\Delta t^2(\frac{1}{2} - \tau) D_i^2 n_i^{eq}(x_a,t) \tag{3.40}$$

Using the previously defined definitions for mass and momentum we can write for density

$$\sum_i m n_i = \rho \tag{3.41}$$

mass flux

$$\sum_i m c e_{ia} n_i = j_a \tag{3.42}$$

and for higher orders

$$\sum_i mc^2 e_{ia} e_{ib} n_i = j_{ab} \tag{3.43}$$

and

$$\sum_i mc^3 e_{ia} e_{ib} e_{i\gamma} n_i = j_{ab\gamma} \tag{3.44}$$

Substituting this into the second order expansion $n_i^{(2)}$ we gain for the zeroth moment

$$\partial_t \rho + \partial_a j_a = (\tau - 1/2)\Delta t(\partial_t^2 \rho + 2\partial_t \partial_a j_a + \partial_a \partial_b j_{ab}) + O(\Delta t^2) \tag{3.45}$$

And for the first moment

$$\partial_a j_a + \partial_b j_{ab} = (\tau - 1/2)\Delta t(\partial_t^2 j_a + 2\partial_t \partial_a j_{ab} + \partial_b \partial_\gamma j_{ab\gamma}) + O(\Delta t^2) \tag{3.46}$$

The first moment can them be substituted into the zeroth by noticing that $\partial_t^2 \rho + 2\partial_t \partial_a j_a + \partial_a \partial_b j_{ab} = \partial_t(\partial_t \rho + \partial_a j_a) + \partial_a(\partial_t j_a + \partial_b j_{ab})$ which gives the continuity equation to order $\Delta t^2$

$$\partial_t \rho + \partial_a j_a = 0 + O(\Delta t^2) \tag{3.47}$$

For the first order equation (the momentum equation) we assume that the $O(\Delta t)$ terms are close to zero which leaves

$$\partial_a j_a + \partial_b j_{ab} = (\tau - 1/2)\Delta t(\partial_t \partial_a j_{ab} + \partial_b \partial_\gamma j_{ab\gamma}) + O(\Delta t^2) \tag{3.48}$$

The tensors $j_{ab}$ and $j_{ab\gamma}$ can be determined for the case of the discrete grid. Starting with

$$\sum_i e_{ia} e_{ib} = 3\delta_{ab} \tag{3.49}$$

$$\sum_i e_{ia} e_{ib} e_{i\gamma} e_{i\nu} = \frac{3}{4}(\delta_a \delta\gamma\nu + \delta_b \delta a\gamma + \delta_\gamma \delta ab) \tag{3.50}$$

Substituting this yields

$$j_{ab} = \rho u_{ia} u_{ib} + P\delta_{ab} \tag{3.51}$$

where $P$ the pressure is determined from the ideal gas law. For $j_{ab\gamma}$

$$j_{ab\gamma} = \rho\frac{c^2}{3}(u_a\delta_{b\gamma} + u_b\delta_{a\gamma} + u_\gamma\delta_{ab}) \tag{3.52}$$

Substituting gives

$$\partial_a j_a + \partial_b j_{ab} = (\tau - 1/2)\Delta t(\partial_t\partial_a(\rho u_{ia}u_{ib} + P\delta_{ab}) + \partial_b\partial_\gamma(\rho\frac{c^2}{3}(u_a\delta_{b\gamma} + u_b\delta_{a\gamma} + u_\gamma\delta_{ab}))) + O(\Delta t^2) \tag{3.53}$$

which can be rewritten in vector notation as

$$\partial_a j_a + \partial_b j_{ab} = (\tau - 1/2)\Delta t(\nabla(\frac{\partial P}{\partial t}) + \rho\nabla\cdot(\frac{\partial uu}{\partial t}) + \rho\frac{c^2}{3}\nabla u^2) + O(\Delta t^2) \tag{3.54}$$

If the viscosity is now set as

$$\nu = \frac{2\tau - 1}{6}\frac{\Delta x^2}{\Delta t} \tag{3.55}$$

Then we recover the traditional Navier-Stokes equations (assuming corrections beyond $O(\Delta t^2)$ are ignored).

## Incompressability

The lattice Boltzmann model is itself only pseudo-incompressible. That is to say that compressible is an integral part of the model and true incompressibility cannot be physically achieved. However, in most cases we do not necessarily wish to achieve incompressiblity but rather we require that the divergence of the velocity field is zero. This is fairly trivial to accomplish within the lattice Boltzmann model but since the density still changes we call this pseudo-incompressiblity since it is not truly incompressible. Various incompressible modifications to the lattice Boltmann model have been derived to ensure a divergence free velocity field [10]. Velocity is assumed to be independent of the density

$$\mathbf{u} = \sum_i n_i\mathbf{e}_i \tag{3.56}$$

This ensures the velocity field remains divergence free.
In addition the equilibrium distribution is modified to

$$n_i^{eq} = w_i(\rho + \frac{3e_{ia}u_a}{c^2} + \frac{9e_{ia}e_{ib}u_a u_b}{2c^4} - \frac{3u_a u_a}{2c^2}) \tag{3.57}$$

## Boundary Conditions

Fluid flow is strongly determined by the boundary conditions. In most systems solid boundaries force the fluid velocity to zero as the boundary is approached, such zero velocity boundaries are often referred to as no-slip boundaries. Slip boundaries do occur in rare special cases such as and are still an ongoing area of research [23].

Boundary conditions are the most challenging part of the lattice Boltzmann model. Often they the determination of unknown values for streaming functions using educated guesses or in some cases relying on other numerical techniques to solve the unknowns. The implementation of boundary conditions is therefore the most unstable part of the simulation and since everything about the flow development is determined by these conditions a great deal of care must be taken in order to avoid inaccuracy. There are many different methods for recreating each type of boundary conditions and each has its advantages and drawbacks depending upon its simplicity, numerical workload, accuracy and stability.

No-slip boundaries are the most important type of boundary condition that we face within this work since the solid-fluid interface is our area of study. The most simple type of no-slip boundary within the lattice Boltzmann method is the bounce back boundary.

### Bounce-back

The implementation of the bounce-back rule occurs at the end of the time step. After the system has been relaxed to equilibrium the particle functions which have entered a boundary are reversed in direction so that during the following time step they leave the bound along the path which they entered i.e they are bounced back. For example the function $f_1$ will be bounded back in the opposite direction which is equivalent to interchanging functions $f1$ and $f3$ within the boundary. Other directional pairs will be reversed in a similar manner. The bounce-back

rules recreate the macroscopic no-slip boundary conditions and do so whilst conserving physical laws of mass, momentum and energy conservation. The rules are also very simple to implement and computationally inexpensive often using an insignificant amount of time to compute when compared to the rest of the simulation. The biggest drawback of the bounceback rule is the lack in rates of convergence for increasing resolution which has been shown to be sub-linear [6] of order 1.

### Open

Open boundary conditions (inflow and outflow) are required to simulate the majority of real life physical systems. The typical setup is one of constant flux with a specific velocity profile for the inflow and either a no flux $\partial_n u = 0$ (where n is normal to the outlet) or constant pressure boundary at the outlet. Implimenting an inflow condition is relatively straitforwards. Here the particle functions $n_i$ are simply set the their equilibrium values corresponding to the prescribed velocity and density profile. For the outlet, a more complex setup is needed since many of the incoming particle functions are unknown and must therefore be determined from known functions. To start with outgoing populations are replaced with their equilibrium values, for a 2D lattice Boltzmann model with 9 directions we can then write the outgoing and ingoing fluxes as

$$J_{out} = n_1 + n_5 + n_8 = \rho/24(6 + 12u)$$
$$J_{in} = n_3 + n_6 + n_7 = r\rho/24(6 - 12u)$$

Zero flux is achieved when the outgoing and ingoing flux values are equal, i.e. $J_{out} - J_{in} = 0$ This gives the following value for $r$

$$r = \frac{1 + 2u - 4u_{in}}{1 - 2u} \tag{3.58}$$

### Periodic

Periodic boundaries are the most simple to implement. In exactly the same way for all other numerical schemes the implementation of periodic conditions simply

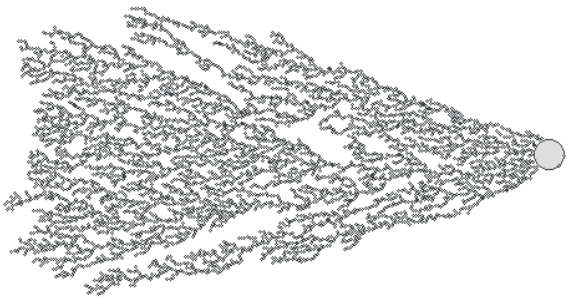

Figure 3.4: Aggregated structure formed from growth on a single nucleation point with free-moving particles following a ballistic trajectory with motion in one direction

requires that all variables leaving one end of the system simultaneously enter the other end.

## 3.3 Aggregation model

Aggregation models represent some of our first attempts to create numerical simulations. The earliest examples include Vold's pioneering ballistic deposition model first undertaken in the 1960s [30] and Sutherland's work in the same field a few years later [26]. Although very simplistic these works later inspired several algorithms most notable from Julien and Meaken (e.g. [12]) who brought the models into the mainstream. These models work by placing particles one at a time upon a structure of previously placed particles in a position which represents the most stable position in the local vicinity of impact. This is achieved by first moving the particle to the surface along its trajectory until impact and then relaxing the particle, usually by moving it along the steepest decent, until the most stable position is found. Particles are usually initiated at a random position above the solid and then moved, often along a specific trajectory, until contact

with the structure. Using these models as tools a great deal of work has been done to investigate the structures formed as certain parameters are varied. From a single seed where particles are randomly aggregated at all orientations, complex branching structures are formed whose form was accurately described in terms of fractal geometry [17]. When particles are given a certain trajectory all along a specific direction before aggregating upon a wall long filamented branching grows from the wall towards the oncoming particles [20]. Investigation into this showed that the angle of incidence of incoming particles was directly linked to the angle of growing structures [21, 20]. And if a single nucleation point was introduced for particles all traveling along a specific direction, large fan-like structures were produced whose shape and angle was determined through geometric calculations [22]. A typical example of such simulations is shown in Figure 3.4. With almost half a century of investigation we have grained great insight into the structures built by ballistic aggregation however, one are of research still lies open and that is the inclusion of fluid flow into the picture.

A simple but accurate aggregation model is presented here to simulate the growth of aggregating structures within a system. Here particles are modeled as hard spheres which collide in-elastically and aggregate with a certain fixed and predetermined probability.

There are two types of particle within the model, free moving particles whose motion is effected by various forces and collisions it experiences and solid particles which maintain a fixed position (solid particles are still involved in collisions but are considered fixed in place). The velocity and position of particles is updated through a simple forward Euler scheme.

Collisions proceed in a classical manner, the classical equation for the collision process can be written as:

$$\mathbf{v}_1' = \mathbf{v}_1 - (1+e)\frac{m_2}{m_1+m_2}\Big((\mathbf{v}_1 - \mathbf{v}_2)\cdot\mathbf{n}\Big)\mathbf{n} \tag{3.59}$$

where $\mathbf{v}$ is the velocity of the particle, $m$ the mass, $\mathbf{n}$ is the normal vector between the two particles and $e$ the elasticity of the collision which ranges from 0 for perfectly inelastic collisions to 1 for perfectly elastic. The prime indicates the new velocity and indicies indicate particle number.

Within the simulation the radius and position of particles are stored to dou-

ble precision. An inaccuracy arises as simulations proceed with a fixed time step whilst the collisions can now occur at any time and will therefore take place at some point in-between two time steps. To correct this particles must be back-tracked to their collision point and then moved with their post collision velocities to accurately position themselves at the end of the time step. The time at which the collision took place can be simply determined from the overlap of the two particles and the pre-collision velocities.

$$t_{collision} = \frac{S}{v_1 - v_2} \tag{3.60}$$

where $S$ the overlap of the particles is $S^2 = (R_1 + R_2)^2 - (p_1 - p_2)^2$, $R$ the particle radius and $p$ the position. Hence the position of the particles at the time of the collision is

$$\mathbf{p}_1' = \mathbf{p}_1 - t_{collision}\mathbf{v}_1 \tag{3.61}$$

and the final position at the time of the current time step is:

$$\mathbf{p}_1'' = \mathbf{p}_1' + t_{collision}\mathbf{v}_1' \tag{3.62}$$

Similar equations exist for particle 2. Aggregation of particles can occur when a free moving particle collides with a solid particle. According to a certain probability the free moving particle will then aggregate becoming a solid particle where its post collision velocity will be set to zero and post collision position will remain fixed.

There is no spacial resolution required for the particle system, however, the time step required careful consideration. In order to prevent particles passing through one another in a single time step (hence avoiding collision when there should have been one, or colliding at the wrong point) the maximum time step must be set to $\Delta t_{max} = R_{min}/u_{max}$, where $R_{min}$ is the minimum particle radius and $/u_{max}$ is the maximum particle velocity.

# Chapter 4

# Precipitation in pipe flow

## 4.1 Paper I and II Overview

The aim of the two published papers [8, 9] was to model a simple precipitation process taking place upon the walls of a pipe where the supersaturated fluid was flowing in order to determine the affects of the main transport mechanisms responsible for the morphology of the growing structure. The model (phase-field coupled with lattice Boltzmann) requires an initial seed to be placed, upon which any further structures grow. From here any variables within the system, in this case Peclet and Reynolds number, could be varied to study their effect. It is important to note that any change of these variables was achieved by altering the magnitude of the diffusion constant and fluid viscosity for $Pe$ and $Re$ respectively. Whilst this is opposite to the most commonly altered attribute in real life situations i.e. the flow rate and hence the fluid velocity, in the case of the model it was simpler and more consistent to alter other parameters.

The initial paper focused upon the growth of a single nucleation site. Here open boundary conditions at the outflow and influx conditions at the inflow represents a situation where supersaturated fluid is constantly pumped from a large reservoir and then removed from the system. In such a system no other structures growing either upstream or downstream are able to add a complex influence upon the growth.

The structures observed to grow within this advected system would consist of one large main dendrite, orientated towards the flow, off which a number of

smaller dendrites would grow most commonly in the upstream direction but also to some extent on the downstream side of the main dendrite.

The angle of asymmetry was defined as the mean angle of the total grown structure with regards to the pipe wall. Here an asymetry angle of $90^\circ$ represents a perfectly symmetric system whilst an angle of $0^\circ$ a perfectly anti-symmetric system where all the growth is on one side. Results showed that for zero $Pe$ number (pure diffusion) the system was completely symmetric (as expected) for low $Pe$ number the angle of asymmetry would reach a minimum whilst as the number increased the angle would decrease once again pushing towards a more symmetric growth morphology. It was determined that advection pushed the fluid at the surface, depleted of solute due to the growth, downstream hence exposing the upstream most part of the growth to fresher fluid and increasing growth rate in this direction whilst simultaneously reducing downstream growth. As the strength of advection increased this area increased in size hence pushing the growth back to a more symmetric state.

Results also showed that as the Reynolds number increased so the asymmetry angle decreased. It was observed that the velocity across the surface would be higher for larger $Re$ numbers hence the advective magnitude at the surface would be greater (even though the mean flow velocity remains the same). At turbulent Reynolds numbers however, a further effect was seen, on the trailing edge of the growing structure turbulent eddies would mix the fluid hence increasing the growth rate in turn slightly reducing the asymmetry.

The second paper investigated a situation where multiple nucleation sites were present in the system causing a complex set of interactions. In a manner identical to the first paper, the first line of study was that of the asymmetry of the growth itself i.e. how much material has grown on one side of the nucleation point relative to the other side. As expected as the advection rate increased so too did the growth rate of the leading edge of the structure hence increasing the asymmetry. However for high $Re$ numbers like in the single dendrite case the opposite started to become true. Here, due to turbulence, as the advection increased the asymmetry decreased and a large quantity of material was observed to grow on the trailing edge of the dendrite. Unlike the single nucleation point however, depleted fluid would become trapped between two adjacent growing structures which significantly reduced the branched growth observed coming off the side of the main dendrite and hence the

majority of dendrites were more symmetric than those in the initial study.

The second area of investigation was the angle between the nucleation point and the tip of the main dendrite which would initially decrease to a minimum for small magnitudes of advection (low $Pe$ number) and then once again increase as the advection was scaled up (increasing $Pe$). As an extension this effect was tested by itself for a very simple setup in which a concentration field was placed around a semi-circular asperity such that the concentration decreased as the surface of the asperity was approached. This setup replicates a snapshot in time of a concentration field with a sink as the surface of the asperity which then undergoes diffusion exactly as is encountered in the initial stages of growth. The concentration field was then advected via a pure Stokes flow ($Re = 0$) such as to track the location of the steepest concentration gradient away from the surface. As Peclet number is the ratio of advection to diffusion the time for which the concentration field was advected in the simple setup was directly equivalent to the Peclet number. This simple setup demonstrated precisely the relationship between $Pe$ number and the angle of the growth confirming the assumptions made about the advective field.

A key part of the paper was to look into the shadowing effects caused by structures growing upstream of others. Advected fluid, slightly depleted from the growth of upstream structures would then reduce the growth of downstream dendrites within a certain distance here referred to as the shadow length. In order to determine this length a number of nucleation sites were placed with every increasing spacing along one wall and ever decreasing spacing along the other. From these two the approximate shadow length could be determined from the shortest distance required before a downstream dendrite appeared unaffected by upstream interference. As one may have expected this length was shown to decrease as the advection rate increased obviously down to the fact that the depleted fluid would be moved a greater distance in the same timeframe. This length was also strongly dependent upon the Reynolds number. For laminar flows, as the Reynolds number increased so too did the shadow length which was determined to be due to large vorticies that formed between sequentially growing structures that trapped depleted fluid diverting it away from downstream structures. For turbulent Reynolds numbers however, the opposite was true and the turbulent field infact enhanced the transport of depleted fluid downstream resulting is a shortening of the shadow length.

Whilst many of the mechanisms involved in the morphology changes are fairly simplistic the paper concludes by noting that turbulence adds significant complexity to the system and, due to its magnitude, this has a significant impact. It was however also noted that the manner in which turbulence is observed to work, as is well known, is as a diffusive field increasing the transport in an isotropic manner. This lead to the next line of work, namely the study of turbulent mixing.

# Chapter 5

# Turbulent dispersion

From the study of precipitation in pipe flow it is quickly apparent that turbulent mixing has a major impact upon the system. Turbulence itself is a truly complex process, described as the last great mystery in classical physics for hundreds of years, in spite of the efforts from the greatest minds in human history we have still failed to unlock all of its secrets. Great progress has however been made within the field. The overall goal is the relate the effects which turbulence has upon the mixing of fluids to variables which a easy to measure in real life such as the flow rate and fluid viscosity. The simplicity is achieved here by relating the mixing caused by turbulence to diffusion through a diffusive constant determined by the turbulent mixing strength which is often referred to as the effective turbulent diffusivity. The starting point here is the turbulent spectrum a defining feature of turbulent motion.

## 5.1 Turbulent spectrum

One of the most important discoveries made within the field of turbulence was that of the energy cascade. Whilst turbulent motion may appear to be totally chaotic and random it does infact consist of coherent structures known as 'eddies'. Eddies are a swirling vortex which derive their energy from shear within the mean flow and subsequently transport it to smaller eddy scales until it is eventually dissipated in what is described as the energy cascade.

There exists several results which are important when studying energy cascades in turbulent flow. Starting from the Navier-Stokes equation we have

$$\frac{\partial \mathbf{u}}{\partial t} + (\mathbf{u} \cdot \nabla)\mathbf{u} = -\frac{1}{\rho}\nabla P + \nu \nabla^2 \mathbf{u} + \mathbf{f} \tag{5.1}$$

$$\nabla \cdot \mathbf{u} = 0 \tag{5.2}$$

where the second equation implies incompressible flow. At this point we also define the kinetic energy per unit mass,

$$E = \frac{1}{2}\sum_i u_i^2 \tag{5.3}$$

where $i$ here indicates the directional component.

By taking the curl of the Navier-Stokes equation and defining the vorticity as $\omega = \nabla \times \mathbf{u}$ the vorticity equation is gained

$$\frac{\partial \omega}{\partial t} = (\nabla \cdot \omega)u + \nu \nabla^2 \omega \tag{5.4}$$

The important term is the first term on the right hand side which defines the process of vortex stretching. When a vortex finds itself within a strain-rate field resulting from velocity gradients, such as that experienced by a small vortex which encounters a larger one, it undergoes stretching. In the direction of positive strain-rate the vorticity is amplified whilst in the negative direction it is reduced. This change is however, not isotropic and it can be shown [27] that the increase in vorticity along the positive strain-rate direction is greater than the decrease along the negative direction, assuming the magnitudes of strain rate are identical. In other words the strain rate field is causing the total vorticity to increase. This vortex stretching therefore involves the transfer of energy where the strain-rate field is doing work upon the vortex.

As the energy is transported down to smaller and smaller eddies the ratio of inviscid forces to viscous forces decreases. This can be seen through the definition of a local Reynolds number $Re = uL/\nu$ where $L$ is now the length scale of the local eddy. Provided the inviscid forces are greater then the viscous forces the eddies themselves do not feel the effect of viscosity. However, at the point where

| | |
|---|---|
| Length scale | $\eta = (\nu^3/\epsilon)^{1/4}$ |
| Time scale | $\tau = (\nu/\epsilon)^{1/2}$ |
| Velocity scale | $u = (\nu\epsilon)^{1/4}$ |

$uL < \nu$ the viscous effects take over and cause the contained kinetic energy to be dissipated in the form of thermal energy. This definition can be used to find the smallest scales which exists within a system, first defined by Kolmogorov as:

For the largest scales no theoretical limit exists as to the size of eddies which are possible to create. However, in most cases the maximum size of eddies possible in the system is constrained by the boundaries of the systems domain e.g. in pipe flow it would be the width of the channel. This is the process by which in three-dimensional turbulence energy at large scales is transported to energy at small scales and finally dissipated as heat. A point of equilibrium can be proposed where the energy entering the system at the largest scales is exactly balanced by the energy leaving the system at the smallest scales, $\partial E/\partial t = 0$. If this is the case the amount of energy at each scale of the system must remain constant. Furthermore as the length scales become shorter the details of the large scale motion become less important. To this effect it is proposed that the total energy transfer must be influenced by only two factors, the dissipation rate $\epsilon$ and the viscosity. This can be used to write the energy in non-dimensional form

$$\frac{E(k)}{\nu^{5/4}\epsilon^{1/4}} = \frac{E(k)}{v^2\eta} = f(k\eta) \tag{5.5}$$

By applying dimensional annalysis to this we gain the form for the law by which the cascade scales

$$E(k) = \epsilon^{2/3}k^{-5/3}f(k\eta) \tag{5.6}$$

The dissipation rate with regards to length scale can also be calculated. The dissipation rate spectrum ($D(k)$) can be defined as

$$\epsilon = \int D(k)dk \tag{5.7}$$

from which we gain

$$D(k) = 2\nu k^2 E(k) \tag{5.8}$$

Applying the same dimensional arguments as for the energy spectrum above the result is:

$$D(k) = 2\nu \epsilon^{2/3} k^{1/3} \tag{5.9}$$

which demonstrates that the dissipation rate increases within increasing $k$ so that smaller wavelengths have a higher dissipation rate.

### 5.1.1 2D turbulence

The first thing to note is that two and three-dimensional turbulence, whilst they share similar results, are inherently different in the way they conserve and dissipate various quantities. If we look at the vorticity equation we immediately see the first key difference between two and three-dimensional cases.

$$\frac{\partial \omega}{\partial t} = (\nabla \cdot \omega)u + \nu \nabla^2 \omega \tag{5.10}$$

In the three-dimensional case the first term on the right hand size defines vortex stretching whilst in the two-dimensional case this term is zero. As a result in the invicid case ($\nu = 0$) for two-dimension vorticity is conserved. If this is now translated to energy evolution in two-dimensions we have

$$\frac{dE}{dt} = \frac{1}{2}\frac{d\sum_i u_i^2}{dt} = -\nu Z \tag{5.11}$$

where $Z$ is the enstrophy which is governed by the following equation

$$\frac{DZ}{Dt} = -\nu \mid \nabla \omega \mid^2 \tag{5.12}$$

From these equations we see that we are dealing with vorticity gradients which are enhanced when small patches of vorticity are stretched by the background vorticity. Again these gradients are able to increase until the viscosity dominates at small scales which acts in a manner that smooths out the system. This is similar for the three dimensional case for the energy but here we are instead working with

the enstrophy. This process occurs both in two and three-dimensions however, the key difference is that whilst in the three-dimensional case the enstrophy increases with time in two dimensions it is forced to decrease. In addition we see that in two-dimensions it is possible for the energy to be conserved in the inviscid limit whilst in three-dimensions the energy decreases at a constant rate. This conservation of energy in the inviscid limit leads to an inability for two-dimensional turbulence to dissipate energy at the smallest scale. Without an energy sink at the smallest scale a direct energy cascade is not possible. Rather then this it has been found [13] that energy instead undergoes an inverse-cascade where energy is transported up the scale and is dissipated due to friction. Enstrophy however is able to dissipate at the smallest scale which causes the direct enstrophy cascade that often defines two-dimension turbulence. To this extent we are able to determine the scaling laws which would be expected for the energy spectrum based upon the enstrophy cascade. We can define the enstrophy dissipation rate as $\eta$ and then defining the relation between enstrophy and energy we have:

$$E_{ns}(k) = k^2 E(k) \tag{5.13}$$

From this we combine the entrophy dissipation rate for which the relationship to the energy dissipation rate is $\nu = \eta/\nu$ and hence $\nu = t^3$ which, through dimensional analysis, gives the enstrophy scaling as:

$$E_{ns}(k) = \nu^{2/3} k^{-3} \tag{5.14}$$

### 5.1.2 Lagrangian spectrum

When dealing with particle statistics rather then fixed measurements one finds oneself in the moving frame of the particle known as the Lagrangian space. Converting between the Lagrangian and Eularian is not always trivial but can be achieved theoretically for the forwards energy cascade. Defining the Lagrangian spectrum as $\phi$ we can write the relationship between Lagrangian and Eularian reference frames as

$$kE = \omega\phi \tag{5.15}$$

Using correspondence between wavenumber and angular frequency $\omega \propto \epsilon^{1/3} k^{2/3}$ and substituting for the Eularian spectrum we acquire $\phi$ as

$$\phi = \epsilon \omega^{-2} \tag{5.16}$$

For the enstrophy cascade we are unable to make this equivalence since the frequence depends only upon the enstrophy dissipation rate as $\omega = \eta^{1/3}$.

## 5.2 Taylor's theory

We wish to determine the effective diffusivity both along and perpendicular to the flow direction within a pipe. Using the flow profile it is possible to determine the rate of momentum transfer which turbulent flow applies within a pipe. An effective diffusivity can then be inferred by relating the rate of momentum transfer to the rate of mass transfer. To this end we begin by stating the relationship between transfer of various properties (mass, energy, momentum) within the flow. In this case we choose to employ Reynolds analogy, this is accurate for very turbulent pipe flow (although the analogy begins to break down in the transitional region). The Reynolds analogy reads as follows:

$$\epsilon = \frac{\tau}{\rho du/dy} = \frac{q}{dC/dy} \tag{5.17}$$

where $\epsilon$ is the coefficient of transfer, $\tau$ is the shear stress and $q$ is the rate of transfer of matter of concentration field $C$

### 5.2.1 Transverse dispersion

We can rewrite Reynolds analogy to make the diffusion coefficient more obvious:

$$q = \epsilon \frac{dC}{dy} = \frac{\tau}{\rho du/dy} \frac{dC}{dy} \tag{5.18}$$

Using this form of the Reynolds analogy the coefficient of diffusion in the transverse direction is simply $\epsilon$ or rather

$$\epsilon = \frac{\tau}{\rho du/dy} \tag{5.19}$$

We, however, are interested in the full system or in other words the integral of $k$ over the width of the channel, to this extent we write:

$$D_{eff_y} = \int_0^W \epsilon dy = \int_0^W \frac{\tau}{\rho(du/dy)} dy \tag{5.20}$$

where $D_{eff_y}$ is the diffusion coefficient in the $y$ direction and $W$ is the width of the channel. In general the velocity distribution $u$ for the pipe can be written as.

$$u = u_0 + \left(\frac{\tau_0}{\rho}\right)^{1/2} f(y) \tag{5.21}$$

where $f(y)$ and $\tau_0$, the flow profile and wall shear stress are dependent upon the Reynolds number and the pipe roughness and are usually estimated from experimental data, $u_0$ is the max flow velocity. Since we have made no assumptions about the form of these profiles the above expression are valid in the general case.

### 5.2.2 Dispersion along the flow direction

In the $x$ direction dispersion has two components, one resulting from the turbulent motion of the fluid and one from the flow in $x$ direction. We may wish to write

$$D_{eff_x} = D_{turb_x} + D_{flow_x} \tag{5.22}$$

Due to the fact that turbulence can be considered to be isotropic then $D_{turb_x} = D_{turb_y} = D_{eff_y}$ which has been calculated in the previous section. For $D_{flow_x}$ we are now making the assumption that the dispersion caused by the flow within the pipe (due to $u(y)$) can be considered to be diffusive. This assumption is based upon two principles. First, when we transfer to a frame moving with the flow then the mean velocity within the frame is zero. Second, due to the turbulent redistribution of the system in the $y$ direction (perpendicular to the flow) over long

time scales we may consider that any part of the system undergoing redistribution due to the turbulence will spend (approximately) equal amounts of time at every $y$ position within the pipe width. This means a particle will spend an equal amount of time moving forwards and backwards in a manner that approximates a random walk. To solve this we shall now make the assumption that $D_{turb_x}$ and $D_{flow_x}$ are independent of one another which means we can determine $D_{flow_x}$ To this end we must solve the full advection diffusion equation which governs the redistribution of mass within the system. Since there is only flow in the $x$ direction this is written as (for simplification we are making the assumption that the fluid is incompressible and hence divergence free):

$$\frac{\partial C}{\partial t} = -u\frac{\partial C}{\partial x} + \nabla \cdot (\epsilon \nabla C) \tag{5.23}$$

We seek to evaluate this from the point of center of mass and hence we must transfer to a frame moving with the mean flow. The transform is defined as follows.

$$x' = x - Ut \tag{5.24}$$
$$y' = y \tag{5.25}$$
$$t' = t \tag{5.26}$$

where $U$, the mean flow velocity, can be calculated from the velocity profile (previously stated) as.

$$U = \int_0^W (u_0 + \left(\frac{\tau_0}{\rho}\right)^{1/2} f(y))dy \tag{5.27}$$

The advection diffusion equation in moving coordinates reads

$$\frac{\partial C}{\partial t'} - U\frac{\partial C}{\partial x'} = -u\frac{\partial C}{\partial x'} + \nabla' \cdot (\epsilon \nabla' C) \tag{5.28}$$

where $\nabla' = \frac{\partial}{\partial x'} + \frac{\partial}{\partial y'}$ for the transformed coordinates and $\epsilon = \frac{\tau}{\rho du/dy}$ as previous. We wish to rewrite the equation in a way such that we can determine the value of an effective diffusivity in the $x$ direction which can be determined from Reynolds analogy:

$$q = D_{eff}\frac{\partial C}{\partial x'} \tag{5.29}$$

where $D_{eff} = D_{flow_x}$ is the effective diffusivity due to the flow and does not depend on $C$. $q$, the flux in the $x$ direction due to the flow, is simply

$$q = (U - u)C \tag{5.30}$$

Which means we seek an equation of the form:

$$(U - u)C = D_{eff}\frac{\partial C}{\partial x'} \tag{5.31}$$

Starting from the advection diffusion equation in moving coordinates we make the assumption that the system is in steady state $\partial C/\partial t' = 0$ the equation now reads:

$$(U - u)\frac{\partial C}{\partial x'} = \frac{\partial}{\partial y'}(\epsilon\frac{\partial C}{\partial y'}) \tag{5.32}$$

Note: due to the earlier assumption that $D_{turb_x}$ is independent of $D_{flow_x}$ we can exclude the $k\partial^2 C/\partial x'^2$ term. It should be clear that to acquire an equation in the form $C = a\frac{\partial C}{\partial x'}$ we simply integrate twice with respect to $y$, this gives us

$$C = \int^{y} dy^{'} k^{-1} \int^{y^{'}} dy^{''} \big(U - u(y^{''})\big)\frac{\partial C}{\partial x'} \tag{5.33}$$

We shall then assume that the concentration $C$ can be written as

$$C = C_{x'} + C_{y'} \tag{5.34}$$

so that the derivative of $C$ with respect to $x$ is independent of $y$ and can be moved outside the integral which gives us the result

$$C = \int^{y} \frac{dy^{'}}{\epsilon} \int^{y^{'}} dy^{''} \big(U - u(y^{''})\big)\frac{\partial C_{x'}}{\partial x'} \tag{5.35}$$

The transfer rate of $C$ in the $x$ direction at a point of the channel is then just

$$q = (U - u)C = (U - u)\int^{y} \frac{dy^{'}}{\epsilon} \int^{y^{'}} dy^{''} \big(U - u(y^{''})\big)\frac{\partial C_{x'}}{\partial x'} \tag{5.36}$$

We use $q$ to indicate that this is the transfer at a specific point in the system and not the total flux across the channel which we shall define as $Q$. Hence, to determine the effective diffusivity for the system we simply integrate across the width of the channel so that

$$Q = \int_0^W (U-u)C dy = \Big( \int_0^W D_{eff_x}(y) dy \Big) \frac{\partial C_{x'}}{\partial x'} \tag{5.37}$$

where

$$D_{eff_x}(y) = (U-u) \int^y \frac{dy^{\cdot}}{\epsilon} \int^{y^{\cdot}} dy^{\cdot\cdot} \big( U - u(y^{\cdot\cdot}) \big) \tag{5.38}$$

which gives us the result

$$D_{flow_x} = \int_0^W D_{eff_x}(y) dy \tag{5.39}$$

and the total $x$ diffusivity is as before

$$D_{eff_x} = D_{turb_x} + D_{flow_x} \tag{5.40}$$

## 5.3 Friction factor

The friction factor is a dimensionless number related to the wall shear stress and the mean flow velocity defined as.

$$f = \frac{2\tau}{\rho u^2} \tag{5.41}$$

The rate at which the friction factor scales with regards to Reynolds number and wall roughness has been an area of significant research due to its importance in industrial applications. The most commonly recognized plot of the friction factor is the Moody diagram, derived from experimental data of rough walled pipe flow it neatly demonstrates the true physical laws governing the friction factor. For laminar flow, the scaling is $f \sim Re^{-1}$ whilst for turbulent flows it is $f \sim Re^{-1/4}$, which relaxes to a constant value depending upon the wall roughness. The scaling

law for laminar flow can be derived trivially from the Poiseuille flow profile as.

$$f \sim \frac{64}{Re} \tag{5.42}$$

The form of the equation for the turbulent scaling law has been derived by several authors (e.g. [3]). However, as can be noted from the Colebrook-White equation they do not present the final solution to the scaling laws and often require an iterative technique to solve.

## 5.4 Shear stress from spectrum

Recently [7] an important discovery was made in the field of friction factor laws. By determining the wall shear stress based upon geometric arguments surrounding turbulent eddies in contact with a rough wall a direct relationship was made between the friction factor and the turbulent spectrum. The derivation begins with the argument that the largest possible size of eddy which can be in contact with the wall is equal to the separation of rough elements see. One then begins with the definition that the velocity of eddies of size $s$ is

$$u_s^2 = \int_0^{1/s} E(k)k^2 dk \tag{5.43}$$

We then wish to create an expression for the wall shear stress $\tau$ which is related to the momentum transfer away from the wall as $\tau = \rho V v_n$ where $v_n$ is the velocity normal to the wall. This normal wall velocity is directly related to the velocity of the dominant eddy in contact with the wall which has been determined above from the energy spectrum as $u_s$. The friction factor can then be written as $f = u_s/V$. Rewriting the equation for $u_s$ in non-dimensional form using the Reynolds number and defining $x = kR$ and substituting for the spectrum as $E(k)\ \epsilon^{2/3}k^{-5/3}$

$$f = K(\int_0^{s/R} x^{-1/3} Re^{-3/4}/x dx)^{1/2} \tag{5.44}$$

Which leads to the result that

$$f = K(r/R + aRe^{-3/4})^{1/3} \tag{5.45}$$

From this equation it can quickly be seen how the $Re^{1/4}$ law arises and how the friction factor relaxes to a constant value based upon the wall roughness. This theory does, however, make a further prediction which is that the scaling law between friction factor and Reynolds number is determined by the form of the energy spectrum. For the enstrophy cascade which presents itself within 2D flow we can substitute for $E(k) \simeq \eta^{2/3}k^{-3}$ which then provides:

$$f_{ens} = K(r/R + aRe^{-3/2})^{1/3} \tag{5.46}$$

Suggesting that for the enstrophy cascade the friction factor should scale as $f \sim Re^{-1/2}$

## 5.5 Scaling laws

From the above using Taylor's theory, we can derived a relation between the friction factor and the effective diffusivity $D_{eff_x}$. By inserting the assumed form of the velocity profile ($u = u_0 + (\tau_0/\rho)^{1/2} f(y)$) and removing dimensions by setting $z = y/H$, we acquire an equation of the following form:

$$D_{eff_x} = \left(\frac{\tau}{\rho}\right)^{1/2} HF(z) \tag{5.47}$$

where $F(z)$ is a function based upon the velocity profile. This then provides the approximate relation between effective diffusivity and friction factor as

$$f \sim \left(\frac{D_{eff_x}}{HU}\right)^2 \tag{5.48}$$

Here is an equation relating the friction factor to the effective diffusivity of a cloud of particles undergoing dispersion due to turbulence within a mean flow. Further an equation relating the friction factor to the Reynolds number and the wall roughness has been derived trough its relation to the energy spectrum. Coupling these

all together we acquire the final form for the scaling law linking Effective diffusivity and Reynolds number as:

$$D_{eff_x} \sim Re^{-1/8} \tag{5.49}$$

for the energy cascade as $r/H \to 0$.

$$D_{eff_x} \sim (r/H)^{1/6} \tag{5.50}$$

as $Re \to \infty$. And

$$D_{eff_x} \sim Re^{-1/4} \tag{5.51}$$

for the enstrophy cascade as $r/H \to 0$.

$$D_{eff_x} \sim (r/H)^{1/2} \tag{5.52}$$

as $Re \to \infty$.

Note: we are unable to make a true dimensional analysis with regards to both $Re$ and $r/R$ due to the dependence of the integrals on the profile of velocity.

## 5.6 Paper III Overview

With the derivation of the expected scalings relations the aim was to determine if these truly present themselves within a real system. What was most important was to show that different types of turbulent spectra produce different scaling laws which can only be achived if 2D systems are considered where both the enstrophy and energy cascades are present. If this were to be done through experiments (and it should be to form a more vigorous proof) then 2D flows can be achieved through soap film flows [16]. Here a soap film is suspended between a series of thin wires and gravity is used to drive the flow in a specific direction. Such flows can be seeded either with finite particles or with a dye from which the dispersion can be measured. However, such experiments are tremendously time consuming and so to gain a good initial verification simulations are turned to. The most important part of this theory occurs in suggesting that every scale of the turbulent cascade contributes to the value of the wall shear, and small scales here near the wall

hold considerable importance. As a result of this the entire range of scales for any turbulent motion which is to be investigated must be simulated, this is often referred to as Direct Numerical Simulation (DNS). Determining the dispersion requires a simple seeding of the flow with passive tracers which follow the fluid streamlines as precisely as possible. From these tracers the position over time can be used to calculate $< x^2 >$ and hence the effective diffusivity.

Different geometry types are employed in order to achieve the two different cascade types within a 2D flow. For the standard energy cascade a rough wall is used whilst for the enstrophy cascade a grid is placed at the entrance to the channel.

The resolution of the simulation held great importance. For the results to be accurate it had to be such that an increase in resolution would not have a significant effect upon the results. To this end, a series of simulations at ever increasing resolution were run and a number of parameters including the velocity field, the density/pressure field, the position of the particles and finally the output effective diffusivity were compared relative to one another. This occurred at $Re$ 6000, 30,000 and 60,000 which produced the appropriate resolution brackets so for example a simulation of $Re$ 50,000 would be run at the resolution determined for 60,000.

One thing that needs to be avoided is any possibility of resonance which could occur within simulations, most notable in the case of the rough wall, due to the ease of creating a regular geometry. For this reason a random spacing is selected with an average equivalent to the spacing aimed for. In this case rough walls were implemented as a series of semi-circles upon the wall. The flow was initially set to a pure laminar profile after which turbulence, generated via the geometry, was allowed to reach steady state. A spacing was selected based on a series of simulations where the time frame in which turbulence reached steady state was investigated. The appropriate geometry was then one which caused turbulent motion to reach a steady state in the shortest amount of time so as to keep the simulation time to a minimum. A similar set of simulations was run to test the grid geometry, this time however, the most appropriate grid was selected based upon how much drag it caused on the flow whilst still producing the desired turbulence. Once the geometries were selected the same geometries were run for all Reynolds numbers for a more accurate and direct comparison of the scaling laws regarding $Re$

number without any inadvertent geometric affects.

The work then proceeded to calculate the produced scaling laws. One thing that became apparent very quickly was that the scaling laws for rough wall turbulence followed a $Re^{-1}$ (approximate) relation up to very high Reynolds numbers. This scaling law is expected only for laminar flow a law that is not possible to recover based upon theory. Whilst no law could be predicted by the theory for laminar flow that does not exclude the fact that some law may still exist and that for some reason the transition to turbulence in the system was simply occurring at a much higher Reynolds number than expected. The most likely reason for this was based upon the geometry being too smooth as the apparent transition to turbulence for the grid geometry was exactly as expected and hence a much rougher geometry was run as a test. However this rough geometry gave the same transition point suggesting that the flow itself was not laminar. From a more simple test it was then determined that the appropriate diffusivity in the x-direction would only be recovered if the magnitude of turbulence were great enough to override the displacement caused by the mean flow and produce the apparent random walk motion associated with diffusion. Whilst these tests were very crude they did indicate that the turbulent motion within the simulations was close to the limit especially for lower Reynolds number and hence despite the flow being turbulent the dispersion in the x-direction would only be semi-diffusive and would not therefore produce the laws sought after.

In addition to investigating the scaling laws this model also allowed the measurement of the Lagrangian velocity field (from the point of view of the moving particles) and hence the Lagrangian spectrum. This is a spectrum that thus far has undergone very little research[1] and whilst mathematically we can predict the scaling for the energy cascade we are unable to do so for the enstrophy cascade.

1. It is odd that so little is known (or in the least published) about the Lagrangian spectrum in the enstrophy cascade. Atmospheric flows on a global scale are two dimensional in nature and many of the measurements of such flows are undertaken by objects that move with the flow such as instrument bearing balloons.

# Chapter 6

# Ballistic aggregation

## 6.1 Field samples

In order to check the results output from numerical models, one requires true life physical examples. Located in Hengill, Iceland the Hellisheidi power plant is the third largest geothermal power station in the world. The geothermal power plant pumps geothermal fluid from a depth of up to 3000m up through a number of production wells. This fluid has a temperature of up to 300 degrees and is rich with desolved silica which precipitates within the pipelines. Silica precipitation samples were collected using stainless steel plates measuring 5 x 2.5 cm. The plates were suspended within the flow using steel rods placing them close to the center of the channel. The samples were left within the pipe for 6-8 weeks before being extracted and dried.

### 6.1.1 Plant schematic

### 6.1.2 Samples

The precipitated structures formed upon the plates varied significantly between the sampling points. Precipitation upon plate (1) produced fan shaped structures orientated towards the oncoming flow. These fans averaged at about 2mm in size. Plate (2) located immediately after the heat exchanger showed little in the way of solid structure. Upon the surface of the plates however wave-like patterns of silica

formed, whilst there is still some discussion it is believed that these structures formed as the silica rich fluid dried upon the surface of the plates. Plate (3) located further downstream of plate (2) had little or no silica upon the surface. Plate (4) was located immediately downstream of the condensate exchange. The plate showed a buildup of flakes upon the surface which form a hexagonal pattern with raised edges where two or more flakes have clearly grown into one another. This plate is still a curiosity as growing structures show no preferred direction but rather grow symmetrically out from what is thought to be an initial nucleation point. The most likely explanation for this is that due to the steam the plate may be growing within a more gaseous environment whereby steam condenses upon the plate and spreads symmetrically hence forming the observed structures. Plate (5) was located just before the injection well and experienced the most growth of all the plates. Have a series of parallel crests seem to form again orientated towards the flow. This is thought to be a more advanced stage of growth similar to plate (1) where the fan-like structures have simply merged to form a single coherent structure.

### 6.1.3 Samples under the electron microscope

Under the electron microscope the growth structures reveal some very interesting and slightly unexpected properties. Rather then the structures consisting of a solid continuous precipitate thay instead consist of individual silica spheres which appear to be cemented together to form the observed structures. It is not uncommon for solid precipitate spheres to form within the bulk of a supersaturated fluid [24]. Once formed, such particles will then undergo ballistic aggregation whereby they will stick to one another to form larger structures. Such aggregation is able to occur both within the flow and upon structures rooted to the walls bounding the flow, the only important requirement is a solid surface. It is most likely that the probability of silica precipitates sticking to other silica precipitates is higher than the probability of sticking to steel (or any other solid). Hence the reason why the fan-like structures observed appear to originate from a small number of nucleation points.

## 6.2 Paper IV Overview

From the analysis of the samples several key results are outlined for investigation. First, the structures are made up of a number of individual silica spheres and are not a continuous structure as would be expected from pure precipitation. Second, after analysis of particles filtered from the bulk flow and comparing to the grown structures it is clear that the particles in the structures are on average larger ($20\mu$m) than those which flow in the bulk ($2\mu$m). Finally, the structures produced resemble fans with an orientation pointing towards the flow. From these details it is concluded that silica particles form in the bulk due to precipitation (something which has been previously observed and explained [22]) after which they undergo a ballistic aggregation process in which they collide and stick together eventually forming larger structures.

Two forces were identified within the system as providing the greatest influence upon the trajectory of the particles and hence the morphology of the structures produced by aggregation. These forces were gravity and drag. Whilst gravity always acts to pull a particle downwards with equal force the drag resulting from the movement of the spherical particles through a fluid acts in a manner to equalize the velocity of the particles with the velocity of the fluid. In this manner drag attempts to force a particle to move along the fluid streamlines its success depending upon the magnitude of the force. By substituting the mass of each particle based upon its volume and mass density $m = 3/4R^3\rho$ it can be found that the terminal velocity in the downwards direction caused by gravity and drag within a stationary fluid is

$$\frac{2(\rho - \rho_f)R^2 g}{9\eta} \tag{6.1}$$

In addition, the acceleration of a particle caused by the bulk flow of a moving fluid can be written as

$$\frac{dv}{dt} = -\frac{9\eta}{\rho R^2}\left(v - u\right). \tag{6.2}$$

The key variable here $R^2\rho$ shows that increasing the mass of the particle either by increasing its size or mass density results in a smaller drag force hence heavier particles will fall faster due to gravity will be less influenced by the flow. The aim of the paper was then to scale the mass of the particle to determine what

impact this would have upon the growing structure. It was decided that the easiest parameter to vary was the density of the particles due to the limit computer power placed upon the area of simulation so that larger particles would require more time to simulate. The results showed that as the mass of particles increased and fell faster towards the lower plate so the aggregation rate increased. Heavy fast falling particles would also move more directly towards the plate causing a layer of particle to quickly form upon the boundary upon which further growth occurred. This resulted in a situation very similar to previous studues where growth occurs over a large area rather than from a single nucleation point forming a number of competing branching dendrites which grow towards the incident particles. For very low particle masses the drag force was so great that particles followed the fluid streamlines closely. Since the flow always acts in manner as to move around any solid obstacles in its path any particles closely following the flow would be diverted around and away from the aggregating structure hence reducing the chance of collision and hindering the growth rate. Collision would only occur for particles very close the the boundary where, due to the no-slip conditions, the flow would only creep causing particles to accumulate in the region resulting in a thin layer of growth across the surface of the boundary. In between these two extremes fan-like structures similar to those observed would grow. Within the actual system it is most likely that due to the size and mass density of silica particles the influence of flow would be high whilst the influence of gravity would be low. In this case the simulations suggest only a thin layer of particles should form upon the plates surface. However due to the variation of sizes, larger particles, less influenced by flow and more influenced by gravity, would not only be more likely to aggregate but also more likely to form the types of fan-like structures observed. In this way flow acts to filter out the large particles which would explain why particles collected from the bulk were on average smaller then those making upo the aggregated structures. The final simulation tested the case of a polydisperse system which resulted in a growth very similar to those observed and caused a filtration of the larger particles as predicted.

# Chapter 7

# Concluding remarks

The aim of this project was to accurately replicate a variety of surface growth problems within flowing systems that eventually lead to a clogging effect that restricts or stops the flow. This replication would occur via the use of numerical simulations which could then be used to evaluate the effect various mechanisms had upon the system. This evaluation would provide the tools needed to predict the evolution of surface growth and eventual clogging processes.

The first numerical model created and evaluated was that of a precipitation reaction in flow achieved using a phase-field model for the surface growth precipitation and a lattice Boltzmann model for the flow. The case of a single structure growing from a nucleation point was initially evaluated followed by the evaluation of a multi nucleation site system. The addition of flow resulted in fan-like structures with a single main dendrite orientated towards the flow upon which a number of smaller branching dendrites would grow mostly on the upstream side of the main dendrite. In all cases it was observed that advection would increase the asymmetry of the system causing more growth towards the flow as supersaturated fluid was initially removed from the upstream most point. Advection would also move this depleted fluid downstream hence hindering growth in this region, a region whose size would depend upon the advective strength. Turbulence was also observed with the system at high enough Reynolds numbers. Eddies, generated by the growing structure, would mix the fluid transporting material towards the surface and enhancing growth in a manner similar to diffusion.

A highlight from the initial study showed that whilst turbulence is complex in

nature it acts in a simple diffusive manner with it own effective diffusivity. Previous work was built upon giving a theoretical prediction for the manner in which the turbulent diffusivity scaled with Reynolds numbers based upon the manner in which energy cascades in a turbulent system. These scalings are $D \sim Re^{-1/4}$ for the direct energy cascade and $D \sim Re^{-1/2}$ for the enstrophy cascade. The lattice Boltzmann model was run in 2D as a DNS for high Reynolds numbers in order to probe these two scaling laws. Whilst some unexpected results were found the scaling laws expected were also reproduced.

A detailed analysis of samples collected from a specific system in Icelend in which precipitation is found to occur within geothermal pipe lines showed that in this system, rather than a pure precipitation reaction occurring, solid spheres would form under precipitation within the bulk flow, after which these particles would then ballistically aggregate to form larger structures. the large structures can be referred to as fan-line with an orientation pointing towards the flow. Further the samples revealed that larger particles are preferentially deposited over smaller ones. A ballistic aggregation model in which passive particles moved by the fluid flow undergo classical collisions with a chance of sticking together is built to simulate the process. The model produced an excellent replication of the structures in the samples. Further, it was also shown that, due to the properties of the flow, acting to divert particles around and away from solid structures, larger particles which are less affected by the flow due to their mass would be more likely to aggregate.

This work should provide a good framework for the general laws which flow-based surface growth adheres to. Further the details of the models can easily be used to simulate more specific systems in future.

# Bibliography


[1] P. L. Bhatnagar, E. P. Gross, and M. Krook. A model for collision processes in gases. i. small amplitude processes in charged and neutral one-component systems. *Phys. Rev.*, 94:511–525, May 1954.

[2] John W Cahn and John E Hilliard. Free energy of a nonuniform system. i. interfacial free energy. *The Journal of chemical physics*, 28(2):258–267, 1958.

[3] Cyril Frank Colebrook. Turbulent flow in pipes, with particular reference to the transition region between the smooth and rough pipe laws. *Journal of the ICE*, 11(4):133–156, 1939.

[4] Joseph B Collins and Herbert Levine. Diffuse interface model of diffusion-limited crystal growth. *Physical Review B*, 31(9):6119, 1985.

[5] Uriel Frisch, Dominique d'Humieres, Brosl Hasslacher, Pierre Lallemand, Yves Pomeau, Jean-Pierre Rivet, et al. Lattice gas hydrodynamics in two and three dimensions. *Complex systems*, 1(4):649–707, 1987.

[6] Martha A Gallivan, David R Noble, John G Georgiadis, and Richard O Buckius. An evaluation of the bounce-back boundary condition for lattice boltzmann simulations. *International Journal for Numerical Methods in Fluids*, 25(3):249–263, 1997.

[7] Gustavo Gioia and Pinaki Chakraborty. Turbulent friction in rough pipes and the energy spectrum of the phenomenological theory. *Physical review letters*, 96(4):044502, 2006.

[8] Christopher Hawkins, Luiza Angheluta, Øyvind Hammer, and Bjørn Jamtveit. Precipitation dendrites in channel flow. *Europhysics Letters*, 102(5):54001, 2013.

[9] Christopher Hawkins, Luiza Angheluta, and Bjørn Jamtveit. Hydrodynamic shadowing effect during precipitation of dendrites in channel flow. *Physical Review E*, 89(2):022402, 2014.

[10] Xiaoyi He and Li-Shi Luo. Lattice boltzmann model for the incompressible navier–stokes equation. *Journal of statistical Physics*, 88(3-4):927–944, 1997.

[11] FJ Higuera and J Jimenez. Boltzmann approach to lattice gas simulations. *EPL (Europhysics Letters)*, 9(7):663, 1989.

[12] R Jullien and P Meakin. Simple three-dimensional models for ballistic deposition with restructuring. *EPL (Europhysics Letters)*, 4(12):1385, 1987.

[13] Robert H. Kraichnan. Inertial ranges in two-dimensional turbulence. *Physics of Fluids (1958-1988)*, 10(7):1417–1423, 1967.

[14] JS Langer. Instabilities and pattern formation in crystal growth. *Reviews of Modern Physics*, 52(1):1, 1980.

[15] JS Langer. Models of pattern formation in first-order phase transitions. *Directions In Condensed Matter Physics. Series: Series on Directions in Condensed Matter Physics, ISBN: 978-9971-978-42-6. WORLD SCIENTIFIC, Edited by G Grinstein and G Mazenko, vol. 1, pp. 165-186*, 1:165–186, 1986.

[16] J Lyklema, PC Scholten, and KJ Mysels. Flow in thin liquid films. *The Journal of Physical Chemistry*, 69(1):116–123, 1965.

[17] Benoit B Mandelbrot. *The fractal geometry of nature*. Macmillan, 1983.

[18] Guy R McNamara and Gianluigi Zanetti. Use of the boltzmann equation to simulate lattice-gas automata. *Physical Review Letters*, 61(20):2332, 1988.

[19] Paul Meakin and Bjørn Jamtveit. Geological pattern formation by growth and dissolution in aqueous systems. *Proceedings of the Royal Society of London A: Mathematical, Physical and Engineering Sciences*, 466(2115):659–694, 2010.

[20] Paul Meakin, P Ramanlal, Leonard Michael Sander, and RC Ball. Ballistic deposition on surfaces. *Physical Review A*, 34(6):5091, 1986.

[21] JM Nieuwenhuizen and HBi HAANSTRA. Microfractography of thin films. *Philips Tech Rev*, 27(3):87–91, 1966.

[22] P Ramanlal and LM Sander. Theory of ballistic aggregation. *Physical review letters*, 54(16):1828, 1985.

[23] I.J. Rao and K.R. Rajagopal. The effect of the slip boundary condition on the flow of fluids in a channel. *Acta Mechanica*, 135(3-4):113–126, 1999.

[24] JD Rimstidt and David R Cole. Geothermal mineralization. i. the mechanism of formation of the beowawe, nevada, siliceous sinter deposit. *Am. J. Sci.;(United States)*, 283, 1983.

[25] Henry De Wolf Smyth. *Atomic energy for military purposes*. Princeton University Press, 1945.

[26] David N Sutherland. A theoretical model of floc structure. *Journal of Colloid and Interface Science*, 25(3):373–380, 1967.

[27] H. Tennekes and J.L. Lumley. *A First Course in Turbulence*. Pe Men Book Company, 1972.

[28] B. Hasslacher U. Frisch and Y. Pomeau. *Phys. Rev. Lett.*, 56, 1986.

[29] JD Van der Waals. Thermodynamic theory of capillarity assuming continuous change of density. *Natuurk. Verb. Kon. Akad. Amsterdam*, 1:1–56, 1892.

[30] Marjorie J Vold. Computer simulation of floc formation in a colloidal suspension. *Journal of Colloid Science*, 18(7):684–695, 1963.

[31] Z. Xu and P. Meakin. Phase-field modeling of solute precipitation and dissolution. *The Journal of chemical physics*, 129:014705, 2008.